Optimized Stokes imaging for highly resolved optical speckle fields, Part III: topological analysis of polarimetric state distributions with optimized data representations

Jonathan Staes, Julien Fade

Optimized Stokes imaging for highly resolved optical speckle fields, part III: Topological analysis of polarimetric states distributions with optimized data representations

JONATHAN STAES,[1] AND JULIEN FADE[1,2,*]

[1] *Univ Rennes, CNRS, Institut FOTON - UMR 6082, F-35000 Rennes, France*
[2] *Aix-Marseille Univ, CNRS, Centrale Med, Institut Fresnel, Marseille, France*
[*] *julien.fade@fresnel.fr*

Abstract: In this last article of a three-paper series focusing on Stokes polarimetry of optical speckle fields resolved at the individual speckle grain scale, experimental results are provided on test samples of varying nature and polarization properties, and are analyzed extensively. For this purpose, a review of the classical ways of displaying Stokes polarimetric information is provided. Then, some original alternative graphical representations are introduced that ensure optimal readability and interpretability of the Stokes imaging data in the context of speckle field polarimetry, and it is shown how they can be adapted to various observation scales. Finally, these tools are implemented in order to provide a topological analysis of the distribution of the states of polarization across a speckle pattern, and in the vicinity of polarimetric singularities of the field.

1. Introduction

This article is the third of a paper series titled "Optimized Stokes imaging for highly resolved optical speckle fields". After having detailed an optimized experimental Stokes polarimetric imaging setup resolved at the speckle grain scale in the first article of the series [1], we have analyzed in the second article [2] optimum acquisition and processing strategies which can be implemented to estimate the polarimetric state with the best accuracy, precision, and robustness to experimental imperfections. In this last paper, we present a set of experimental results that have been acquired with this setup and these optimized acquisition/processing modalities. In addition, we propose original graphical representations of the polarimetric information measured, and we discuss their relevance according to the various scales of observation of the speckle patterns that we analyze. This discussion about the choice of a relevant representation as a function of the scale of analysis is finally illustrated through several analyses of the "topological" behaviour of the state of polarization (SOP) across a speckle field, at the frontier of two speckle grains, or in the vicinity of polarization singularities of the speckle field.

This paper is organized as follows: in Section 2, we report the experiments conducted and results gathered that will be the basis of discussion of all the remainder of the article, and we provide a first global polarimetric analysis of these results. Then, we propose and compare in Section 3 various modalities of graphical representation of polarimetric information. We discuss their respective relevance for better visual understanding of the physical situation at hand, since producing a legible two-dimensional graphic representation that displays as well as possible such a 6-dimensional polarimetric information is not trivial. In Section 4, we provide a thorough analysis of the "topological" behaviour of the distribution of the SoP across a speckle pattern, at various spatial scales (population of grains, neighbouring grains, single grain), using the graphical representations proposed in Section 3 that can be refined and adapted depending on the scale at which the speckle pattern is observed. A similar topological analysis is provided in Section 5 at the vicinity of polarization singularities in a speckle pattern. Finally, a global conclusion and some perspectives of this article series are given in Section 6.

2. Overview of experiments and global polarimetric analysis

This article relies on experimental Stokes imaging acquisitions that have been performed with the imaging setup detailed in the first article of this series [1]. In this first article, we also reported the principle of Stokes polarimetric imaging, as well as the exact final experimental configuration retained after optimization of the acquisition setup. We therefore refer the reader to this first article in order to get more details about these points, and to fix the notations used in the present article. Moreover, the data gathered and discussed here have been obtained and processed according to the optimal acquisition/processing strategy that has been theoretically studied and characterized in the second article of this series [2], namely, the optimized so-called SOPAFP approach detailed and advocated in [2]. For data reproducibility, we invite the reader to refer to these two papers in order to get full details about the acquisition and processing pipelines that have been used.

The experimental results reported and analyzed here were acquired from the polarimetric analysis of speckle pattern obtained upon interaction of a highly coherent single-mode green laser with four samples of varying polarimetric nature, ranging from non-depolarizing to highly depolarizing (see also [1] for more details), namely:

- a metal plate (brushed aluminum), whose polarimetric behaviour is (quasi perfectly) non-depolarizing [1, 3, 4];
- a block of marble painted in green whose partially depolarizing nature is due to a volume scattering regime of the incident green light source (monochromatic at $\lambda = 532$ nm) [3].
- a Spectralon sample exhibiting a highly depolarizing polarimetric behaviour [5–8], coupled with high reflectance (≈99%), and whose strongly Lambertian behaviour is generally used for the calibration of optical instruments [9, 10], particularly in Spectralon-coated integrating spheres.
- a piece of tissue phantom (Polydimethylsiloxane (PDMS) polymer with scattering nanoparticles of titanium dioxide (TiO_2) and absorbing India ink) whose optical behaviour approximates the optical properties of biological tissue [11, 12].

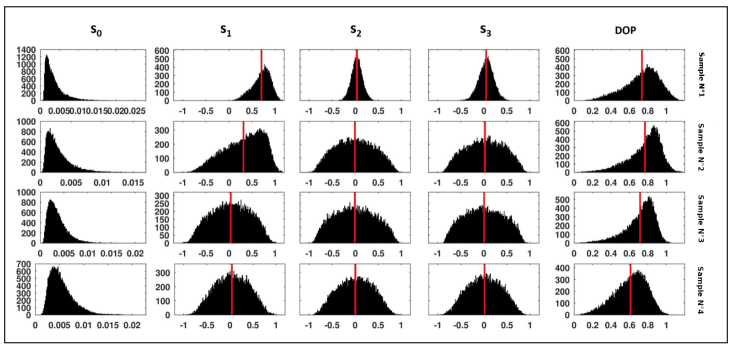

Fig. 1. Histogram of the various Stokes parameters and the degree of polarization for the following samples: metal plate (n°1), brick covered with green paint (n°2), Spectralon (n°3) and PDMS phantom (n°4).

In order to check the polarimetric nature of each sample used in this experimental work, a statistical analysis of the polarization properties of the speckle fields produced on each of these samples is first provided below, at a macroscopic scale, over the whole resolved speckle field. For that purpose, the histogram of the different Stokes parameters for a region of interest (ROI)

of 150×150 superpixels (each superpixel resulting from a 4×4 binning of the pixels of the detector [1]) for each sample is shown in Figure 1. We recall here that the illumination source is vertically polarized, and thus with conventions of [1, 2] the theoretical incident polarization state corresponds to a Stokes vector $\mathbf{S}^{in} = S_{in}\begin{bmatrix}1 & 1 & 0 & 0\end{bmatrix}^T$ with S_{in} the input illumination intensity.

As expected, it can be seen in Fig. 1 that polarization state of the speckle pattern obtained with the metallic sample (sample n°1) basically retains the SOP of the incident laser source, as shown by the mean values of the reduced Stokes parameters s_1, s_2 and s_3, which are respectively equal to 0.704 ± 0.002, 0.035 ± 0.002 and 0.054 ± 0.002, while retaining a high degree of polarization (DOP) when evaluated locally across the speckle field, with an average spatial DOP, denoted $\overline{DOP}$, of 0.736 ± 0.002 (The given precision correspond to the standard deviation of estimation over sets of 150×150 superpixels). In this article, the reduced Stokes parameters s_i ($i = 1, \ldots, 3$) refer to the elements of the Stokes vector normalized by the first Stokes parameter S_0 which represents the total intensity of the field at the observed location (see [1] for more details on notations). The mean values of the s_i and of the DOP indicated above are displayed in the histograms of Fig. 1 with a solid vertical red line.

As noted in previous similar works [3, 13, 14], the SOP of light across a speckle field (when a static sample is illuminated with coherent polarized light) is well defined at each location of the field, i.e., the DOP should be equal to one at each location of the speckle pattern. It can be observed in the top right histogram of Fig. 1 that the distribution of the DOP values differs from the theoretical expected value of 1, as the statistical (spatial) average comprises also the "dark" pixels (corresponding to destructive interferences in the speckle field, i.e., pixels with low values of S_0) for which the estimated SOP cannot be trusted. When the speckle pattern is preliminary thresholded in order to retain only the pixels that have a significantly high level of S_0, the averaged DOP value then tends to one on such a metallic non-depolarizing sample [3].

For the marble brick covered with green paint (sample n° 2), the standard deviation of the parameters s_1, s_2 and s_3 are wider than for the previous sample and the respective mean of each parameter is 0.315 ± 0.003, -0.006 ± 0.003 and 0.025 ± 0.003. The decrease of the mean value of s_1, coupled with an increase in the standard deviation of the s_i parameters corresponds to a "dispersion" of the incident polarimetric state, suggesting that a green diffusive sample acts as a depolarizing material where volume scattering occurs when illuminated with green laser light. Meanwhile, it can be observed by looking at the histogram of the DOP that these experiments confirm again the fact that the SOP is pretty well defined at each location of the field, with a local DOP value remaining close to one, as the average DOP value is 0.767 ± 0.002.

Finally, the Spectralon and tissue phantom samples (samples 3 and 4) share a similar polarimetric behaviour, with the histograms of the three reduced Stokes parameters s_1, s_2 and s_3 showing similar distributions, corresponding to a modification of the incident polarization state resulting in an almost complete loss of the incident polarimetric state used to illuminate the sample. The analysis of the histograms of the DOP for these two samples reveals that on a static depolarizing sample such as Spectralon, the local DOP values remain close to one (0.715 ± 0.002), whereas the distribution tends to show slightly lower values on the PDMS sample 0.612 ± 0.002. We hypothetically attribute such observation to a stronger influence of mechanical and thermal drifts during the acquisition of the intensity images as the PDMS phantom is more deformable than the Spectralon, even though it was thermalized for about twenty minutes before the images were acquired. As a consequence, and since they share comparable behaviour, we rather focus in the remainder of this study on the spectralon sample.

To complete this macroscopic analysis, it is interesting to analyze jointly the histograms of the local DOP (as displayed in the right column of Fig. 1) and their respective mean values $\overline{DOP}$ (red vertical lines), along with the DOP of the average SOP of the light analyzed in the ROI, i.e., the DOP that would have been obtained in a standard polarimetric imaging situation if the

speckle grains of the ROI had been averaged on a single detector (single pixel). In that case, the DOP of the average resulting SOP is denoted $\widetilde{DOP}$ and computed as $\widetilde{DOP} = \left(\overline{s_1}^2 + \overline{s_2}^2 + \overline{s_3}^2\right)^{1/2}$, where $\overline{s_i}$ indicates the spatially averaged mean value of the i^{th} reduced Stokes component. From the experimental results obtained, we get a value of $\widetilde{DOP}$ equal to 0.707 ± 0.002 for the metallic sample, showing its unperfect non-depolarizing nature even when experimental imperfections are accounted for and compensated (see part 1 of this article series [1]). As for the other samples, the value of $\widetilde{DOP}$ is 0.316 ± 0.003 for the green-painted marble and 0.041 ± 0.003 for the Spectralon and 0.046 ± 0.003 for the phantom sample, which is in clear agreement with the expected respectively non-depolarizing/depolarizing nature of the samples studied, and with the results of previous works on similar samples [1, 3, 5]. This again confirms the fact that the depolarization in such samples and with such active coherent polarimetric imaging experiments is due to a spatial average of well-defined SOPs but which are more or less scattered out across the Poincaré's sphere [3].

Such a statistical analysis can provide an interesting insight on the polarimetric nature of the samples, as discussed above and in several anterior works, however, it does not allow any spatial analysis of the distribution of the SOPs, spatially across the speckle field, or across the Poincaré's sphere. Classically, such Stokes imaging results are analyzed by providing the spatial maps of the various Stokes parameters S_i for $i = 0, \ldots, 3$ and of the DOP, as displayed for instance in Fig. 13 of Section 6 of the first article of this series [1]. In the next section, we recall this classical modality of displaying Stokes polarimetric information, but we propose alternative representations that can be of interest depending on the physical situation analyzed and on the spatial scale at which it is observed.

3. Graphical representations of Stokes polarimetric data

A speckle field is a pattern of light intensity varying spatially in two dimensions in the (x, y) plane. At any point in this plane, the polarimetric information is defined and is characterized by a four-dimensional vector, usually the four Stokes parameters, or the set of intensity, polarization azimuth, polarization ellipticity and DOP of the light. Even in a monochromatic situation (using a graylevel camera) such as the one studied in this article series, representing a 4-dimensional information across a plane is a mere challenge that exceeds the capacities of our human senses and mind. As a result, a compromise is necessarily made when representing such data, and the "dimensions" that one must privilege clearly depend on the problem at hand and on the purpose of the imaging experiment.

The most widely used representation consists in showing each polarimetric parameter as a 2D image, thus preserving the spatial information. This is clearly the solution that has to be advocated for most polarization imaging situations, when one wants to increase contrasts, such as in the biomedical or defense domains for instance. We shall refer in the following to such representations as "spatial-structure-preserving representations", which prioritize the readability of the spatial (imaging) information to the detriment of the polarimetric information.

From another standpoint, some specific situations of polarimetric imaging can afford to relegate the spatial distribution of the pixels in the image to the secondary level. In that case, the main information lies in the way the SOP is distributed among the pixels along the "polarization" dimensions. This is clearly the case in our present study of the polarimetric properties of a speckle field, whose spatial structure is relatively poor in terms of interpretable information, as it consists of a complex interference pattern of speckle grains. In such situations, the analysis of the distribution of SOPs is more easily done by plotting them across a Poincaré's sphere for instance. We shall refer in the following to such representations as "spatial-structure-non-preserving representations", which prioritize the readability of the polarimetric information to the detriment of the spatial information.

In the following subsections, we will introduce and describe several alternative graphical

representations, based on the above definitions, which will allow us to propose optimal readability of the Stokes imaging data, depending on the observation scale (grain population, interface between neighbouring grains, single grain). All these representations detailed below are summarized in Table 1.

Table 1. **Graphical representations developed and used according to the desired scale of observation. (PQ: Peirce-Quincuncial projection)**

	"Dimension" of representation	
Observation scale	Spatial	Polarimetric
Population of grains	-S_0, s_1, s_2, s_3 and DOP -Stokes vector RGB color coding -S_0 + polarization ellipses	-Poincaré's sphere mapping -PQ mapping -ROI + thresholding + colour coding of grain membership/boundaries
Neighbouring grains	-S_0, s_1, s_2, s_3 and DOP -Stokes vector RGB color coding -S_0 + polarization ellipses	-Poincaré's sphere mapping -PQ mapping -Triang. ROI + RGB coding of spat. coord. + boundaries color coding
Single grain	-S_0, s_1, s_2, s_3 and DOP -Stokes vector RGB color coding -S_0 + polarization ellipses	-Poincaré's sphere mapping -PQ mapping - ROI/thresholding (+ meshing) + colour coding of polygonal contour

3.1. Polarimetric representations with preserved spatial structure

To understand polarimetric information on top of a spatial information in a 2D-image, we need to encode it visually in the 'dimensions' accessible to our senses (intensity, colour, 3D, etc.) or by using representation devices superimposed on the image (arrows, bars, ellipses, etc.). The answer to this problem is far from being simple and unique, given the variety of polarimetric parameters and measurement techniques, as well as the applications that require specific information. A great deal of work has been done on encoding polarimetric information while preserving certain information that is visible to the human eye [15–17]. We list below some of the available spatial-structure-preserving representations:

- **Set of 2D maps**: This representation enables spatial information to be perfectly preserved, by providing one spatial 2-D map for each polarimetric channel. In our work, these parameters are represented as follows:
  - S_0 : A grayscale colormap is commonly used, corresponding to the standard image obtained with a non-polarimetric grayscale camera.
  - s_1 & s_2 : As those parameters vary between -1 and +1, the representation we propose consists in using a scale whose extreme values show green and fuchsia colours corresponding respectively for the s_1 parameter to a vertical (s_1=1) and horizontal (s_1=-1) polarization and for the s_2 parameter to a polarization of +45° (s_2=1) and $-45°$ (s_2=-1). The saturation of these colours is directly linked to the values of these parameters. Zero values are represented by a white hue.
  - s_3: Similarly to the previous case, the representation of this parameter uses a scale whose extreme values are represented by the colours blue and red, corresponding

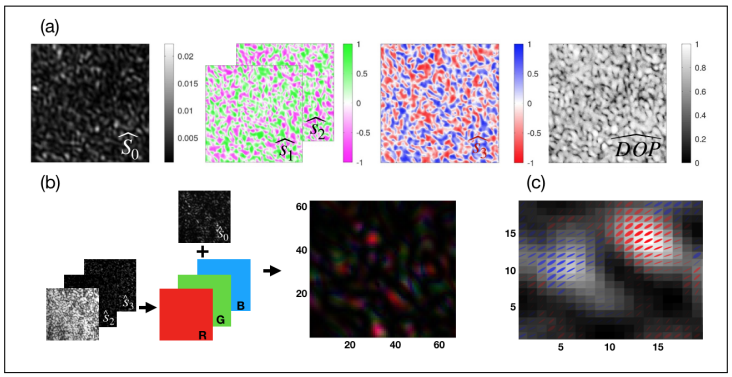

Fig. 2. a) 2D representation of the Stokes parameters: S_0, s_1, s_2 and s_3 as well as the DOP obtained on a Spectralon sample.(b) False colors representation of the polarimetric information (RGB coding with s_1, s_2 and s_3, S_0 encodes the level of luminosity). (c) 2D image of the intensity in graylevels with the polarimetric information implemented as a polarization ellipse in each "superpixel".

respectively to a state of left-circular and right-circular polarization. As with the previous colour scale, intermediate values are represented by a white hue. The different choice of colors (red vs blue) is justified by the fact that these colors will directly indicate the sign of ellipticity of the local SOP in the s_3 map.

– (Optionnally) DOP : Although introducing some redundancy with the above parameters, the DOP map is very commonly used in polarimetric imaging. As it is a scalar bounded between 0 and 1, a grayscale colormap is used, with higher values of the DOP represented by clearer pixels.

The main drawback of this classical representation, which is schematically illustrated in Fig. 2.a on real data, lies in the lack of global interpretability from a single glance, as it requires the joint analysis of 4 to 5 spatial maps (Stokes parameters + DOP).

- **Stokes vector RGB color coding**: This approach, illustrated in Fig. 2.b, is an attempt to summarize all the polarimetric information into a unique map, more suited to visual interpretation. This approach amounts to encoding each SOP into a corresponding colour using an RGB colorimetric encoding (HSV encoding could also be used), obtained from the value of the reduced Stokes parameters s_i, $i = 1, \ldots, 3$. In order to retain the information related to intensity, the brightness of each pixel is linked to the values of the S_0 parameter, i.e., an area of low luminosity is represented by dark colours. Although this representation makes it easier to visualize speckle grains and the spatial evolution of polarization states, it is still inefficient to ensure a clear visual interpretation of the SOP evolution, and then to carry out a careful topological study of the polarization state distribution.

- **Optimized representation: S_0 map + polarization ellipses**: The last representation that we propose in this section consists in visually encoding the SOP on top of the intensity image (S_0 parameter in graylevel) using visual indications that are provided at a lower spatial resolution. This representation, illustrated in 2.c, is inspired from [13] but refined as detailed below to ensure best readability. For that purpose, a layer containing the polarimetric information, consisting of polarimetric ellipses, is superimposed on the intensity image, thereby providing a direct information about the polarization azimuth and ellipticity. A blue (resp. red) ellipse represents a left (resp. right) circular polarization state, with positive (resp. negative) ellipticity. We also propose to encode the polarization

degree in this polarimetric information layer, by linking the "normalized" size of the ellipse to the value of the DOP. For a purely polarized state (DOP=1), the length of the major axis of the ellipse is made equal to the width of the *superpixel*, whereas for a depolarized light, the superimposed ellipse exhibits a vanishing size. A satisfactory magnification scale used on the actual resolution of the S_0 image was shown to be of 16 pixels (i.e., one pixel of the original S_0 is represented with a uniform square of 16×16 pixels, on top of which the corresponding local ellipse is plotted).

This refined representation proves very efficient at quickly visualizing the evolution of the polarization state inside a speckle grain, or across a population of speckle grains. By zooming out on this image, it is also possible to recover a global view of the intensity image without being too much perturbed by the polarization ellipses. For that purpose, we implemented a variable transparency parameter in the display of each ellipse, directly given by the S_0 intensity level. In that way, bright areas (speckle grains) show opaque and clearly visible ellipses, while in dark regions, the ellipses are almost transparent and do not perturb the dark background of the intensity image. Furthermore, this transparency tuning is also directly related to the level of confidence one can expect, as low intensity regions will lead to estimated valued of the Stokes parameters with poor accuracy and precision [2]. This representation, illustrated Fig.2.c, appears to be a good compromise in order to preserve spatial information in an image, while at the same time offering quite clear readability of the polarimteric information on intense pixels. In the present context of Stokes imaging at the speckle grain scale, it can be used at all scales of observation to study the spatial evolution of the SOP and of the DOP.

3.2. Polarimetric representations with non-conserved spatial structure

Polarimetric representations which do not preserve the 2D-spatial structure of the data may be inconceivable in many imaging applications (medical imaging, defence) without impoverishing the interpretability of the results. However, this type of representation can be well indicated to analyze the distribution of polarimetric SOPs in a readable way, making understanding almost immediate once you are familiar with the polarization formalism. In the context of our study, the spatial information is not very informative as noted above, and it becomes acceptable for us to "omit" the spatial structure of the 2D images in favour of a better analysis of the distribution/evolution of the polarimetric states. Thus, in this subsection, we will list some alternative approaches for displaying polarimetric information while improving the readability of the distribution/evolution of the polarimetric states of a speckle pattern at different observation scales.

- **Poincaré's sphere plot**: The Poincaré's sphere representation is a well-known tool allowing all possible polarimetric states to be plotted in a three-dimensional frame of reference which corresponds to the normalized Stokes parameters (s_1, s_2 and s_3). Fully polarized states correspond to the sphere of unit radius, whereas a partially polarized SOP is represented by a point that lie inside this unit radius sphere, its DOP corresponding to the distance of this point to the center of the frame. Using such representation, it is thus possible to map each pixel in a Stokes imaging experiment with its corresponding location in the Poincaré's sphere [3, 14]. An example of such mapping is provided in Fig. 3.a, which shows that in the context of our experiments, the well-defined and polarized SOPs observed at each location of a speckle pattern with sufficiently high intensity correspond to a group of points located at the surface of the Poincaré's sphere. However, the main drawback of such representation lies in its 3-dimensional nature (sphere), preventing the eye from encompassing all possible SOPs with a single glance, which can be the case, as will be seen below with very depolarizing samples, or at the vicinity of polarization singularities.

Furthermore, antipodic SOPs may be superimposed, leading to confusion or occlusion, which can be very annoying on a static representation, such as on a printed 2D figure.

- **Planispheric projections**: An obvious way to circumvent such difficulties is to resort to classical planispheric projection methods, which allow the surface of a sphere to be mapped on a 2D plane. There are tens of planispheric projections that have been proposed with very different properties and characteristics. We can cite here the stereographic projection that has already been proposed to analyze polarization states, and which maps the sphere to a 2D plane [18]. Although such projection has the interesting property of being conformal, it is however barely usable as it maps the sphere to an infinite plane, which also prevents the observer to encompass all SOPs at a time.

- **Preferred representation: Peirce's quincuncial projection**: Among all the alternative planispheric projections at hand, we propose to use the Peirce's quincuncial (PQ) projection [19], which is illustrated in Fig. 3.b. Although we do not detail here the formulation of such projection for the sake of concision, this PQ projection allows all the polarimetric states lying at the surface of the sphere (DOP=1) to be displayed instantaneously on a two-dimensional square map. This conformal map representation is obtained by concatenating eight partial stereographic transformations of the eight octants of the sphere, leading to eight isosceles right triangles forming a square, as shown in Fig. 3.b. The six specific points of coordinates $(1,0,0)$, $(-1,0,0)$, $(0,1,0)$, $(0,-1,0)$, $(0,0,1)$ and $(1,0,-1)$ on the sphere are respectively indicated by letters V, H, P, M, L and R in Fig. 3.b.

  Classically, and as shown in Fig.3.b, the centre of the PS projection corresponds to the north pole of the globe corresponding to the left-hand circular polarization state L on the Poincaré's sphere. In this configuration, the south pole is represented simultaneously in all four corners of the map. The equator of the sphere, corresponding to all the linear states, is shown as a dotted red line on the map (Fig.3.b), forming a diamond shape. For the sake of readability, it can be advantageous to modify the center of the PQ projection, so that it is centered on the average polarization state of the ROI studied, thus improving the readability of the information for the reader. This corresponds to modifying the reference state of the Poincaré's sphere from which the stereographic projection is performed. An example is shown in Fig.3.c, where the center of the map represents the vertical polarization state corresponding to the polarimetric state of the laser source used in the experiment [1]. As can be observed, it also allows to avoid the distorsions caused by the PQ projection when the observed SOPs are located close to the corners of the equator in red (Fig.3.b).

  This PQ projection offers the interesting property of encompassing at a single glance all SOPs, without occlusion or possible confusion between them. Furthermore, it is a conformal projection (except at four singular points on the equator, located at the middle of each vertex of the square), which tends to avoid strong deformations onthe planispheric projection, except at the vicinity of the four singular points on the equator. As a result, in terms of practical use of such projection, we always tended tolegi select a centering point for the projection that minimizes the quantity of SOPs located at the vicinity of these four singular points.

It the remainder of this article, we will analyze the distribution of SOPs across a speckle field using the Poincaré's sphere representation, and with the corresponding PQ projection, which, as will be shown below greatly improves the readability and interpretability of the results. It can be noted here that contrary to the Poincaré's sphere representation, the PQ projection does not directly enable the DOP to be "encoded" in the projected map. This will not be an issue in the context of this study, as the SOP is well defined with a DOP very close to one at any location

of the speckle field under polarized illumination [3, 13, 14]. In a more general context, such additional information could be displayed onto the PQ map using false color coding for instance.

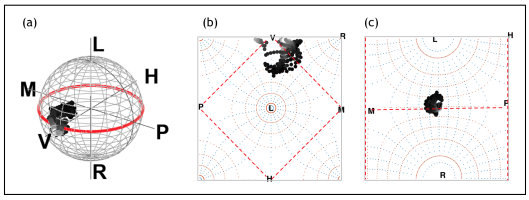

Fig. 3. Representation of the Poincaré's sphere with a distribution of SOPs (a) and its corresponding Peirce's quincuncial projection (b) where the left circular state noted L (+s3 on the Poincaré's sphere) is at the centre of the map. (c) Same as (b) but with a Peirce's projection centered on the linear vertical SOP (corresponding to the illumination state of the laser source in the experiment).

4. Multiscale polarimetric topology analysis of a speckle pattern

In this section, the various representations described above will be used, adapted and refined in order to offer the best interpretability of experimental Stokes imaging results obtained on speckle patterns at distinct scales of observation: grain populations, neighbouring grains and single grain scale. Such multiscale representation tools can indeed prove interesting for upcoming works aiming at analyzing the origin of spatial depolarization of a speckle pattern. We will illustrate below how such experimental data along with optimized polarimetric data representation can lead to interesting observations of the topology of the spatial distribution of SOPs across a speckle field.

4.1. Population of grains

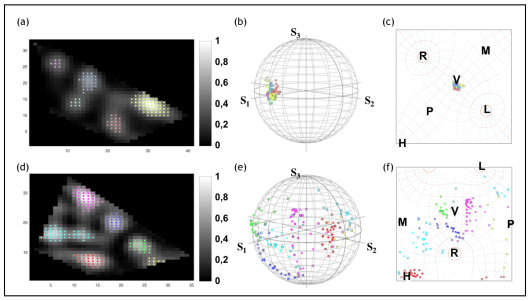

Fig. 4. First column: image of the S_0 parameter with colored markers for the selected pixels. The second column represents the SOPs plotted on the Poincaré's sphere. The last column is the Peirce's projection of the Poincaré's sphere. The first line corresponds to the metal sample and the second to a Spectralon sample.

In this subsection, the aim is to analyze the polarimetric states distribution within speckle grains for a population of grains located in a same selected ROI. As an additional objective, we aim at refining the above data representation strategies, in order to ensure best interpretability of the SOPs distribution, while preserving as much spatial information as possible, although we will resort to "spatial-structure-non-preserving representations" such as Poincaré's sphere and PQ projection.

From the Stokes images acquisition, a ROI is selected using a polygonal contour, as represented in the intensity (S_0) maps in Fig. 4.a and d for two examples acquired respectively on a metallic blade and on a Spectralon sample. A thresholding operation on the values of S_0 enables the brightest pixels in the intensity map to be selected, thereby isolating distinct speckle grains. In order to analyze the spatial distribution of the SOPs across the speckle field, a colour is assigned to each grain detected, and a coloured marker is displayed on each pixel of the grain on the displayed S_0 map, using a magnification scale similar to the one used in Section 4. The colour saturation of each marker is linked to the level of intensity, so that high intensity is represented by a bright colour for readability purpose. All these markers can then be plotted on the Poincaré's sphere (Fig. 4.b and e) and on the PQ projection (Fig. 4.c and f). As a result, using such colored markers makes it possible to distinguish the SOPs of different speckle grains by referring to the reference intensity image (Fig. 4.a and b).

In addition, we wanted to identify in the Poincaré's sphere or in the PQ map the pixels lying on the edge of the speckle grains selected by the thresholding operation. For that purpose, we implemented a black edge on the colored markers corresponding to the pixels belonging to the grain boundary. This makes it possible to visualize the polarimetric state evolution within a grain when it is represented on the Poincaré's sphere and PQ projection.

The two ROIs selected and plotted in Fig. 4 represent a population of grains (<10 grains) of the speckle pattern obtained at the surface of a non-depolarizing sample (polished metal plate) and a highly depolarizing sample (Spectralon), shown respectively in Fig. 4.a and d. It can be seen that all the speckle grains observed on the surface of the non-depolarizing sample have polarization states close to that of the illumination source linearly polarized along the vertical axis (corresponding to reduced Stokes vector $s = [1\ 0\ 0]$) as shown in Figs. 4.b and c. As detailed above, PQ map has been centered on the average polarimetric state, which is close to a state with reduced Stokes vector $(1, 0, 0)$. This observation is clearly in agreement with previous studies [3, 13, 14]

For the Spectralon sample, as expected for a highly depolarizing sample, the SOPs are scattered around the surface of the Poincaré's sphere and the PQ projection (Fig.4.e and f). The polarimetric states observed are distributed over almost all eight octants of the sphere for the six grains analyzed in this ROI. This representation clearly shows that spatial depolarization occurs by the averaging of distinct polarimetric states, but also that each pixel of a speckle grain has a specific distribution of SOP, centered around an average SOP which differs from one grain to the other.

Interestingly, the clear readability of the PQ projection seems to indicate a noticeable property. Indeed, in some situations, a contour which encloses a spatial region in the vicinity of the center of a bright speckle grain seems to be mapped, on the SOP distribution, to a contour on the Poincaré's sphere (or the PQ projection) that encloses the distribution of SOPs of the pixels inside the initial spatial contour. However, as will be discussed later, this property does not seem to be universal for all speckle grains.

4.2. Interface between neighbouring grains

We now propose to focus on the evolution of the SOP in regions corresponding to the interface between neighbouring grains. Two kinds of situations have been analyzed: in the first one we analyze the SOP in a triangular region defined by the centers of the three neighbouring grains. The second situation corresponds to analyze the transition of SOP along a linear trajectory between two grains.

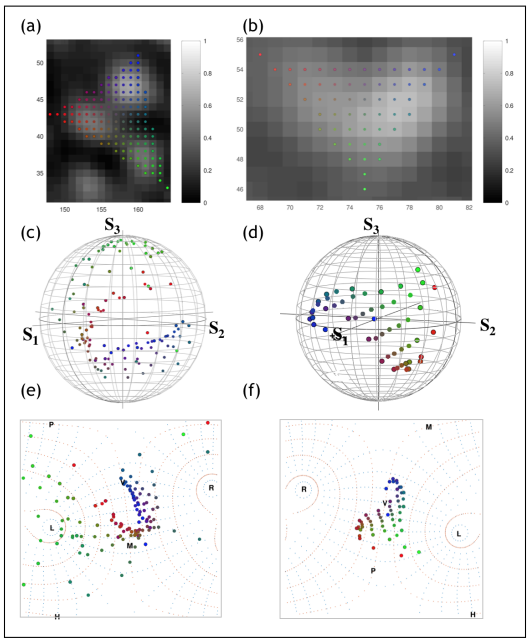

Fig. 5. First column: Representation of the selected ROI on the S_0 image with colored spatial encoding of the pixels locations. Second column: Representation of the Stokes vector at each pixel on the Poincaré's sphere and on the PQ projection, represented in the last column.

Triangular area of interest In order to represent the evolution of the SOP across a triangular area while preserving as much spatial information as possible, we proposed to use colored markers, as introduced in the previous subsection, but with a distinct color encoding. In that case indeed, we assigned the markers colors in such a way that the three triangle summits are respectively assigned a red, green and blue colour, with respective RGB encoding: [1 0 0], [0 1 0] and [0 0 1]. The pixels corresponding to all the other points of the triangle are then assigned a colored marker whose RGB encoding is directly given by the spatial triangular coordinates of the point (while ensuring normalization to 1 of the sum of the RGB values). As a result, the pixel located at the barycentre of the triangular ROI is therefore assigned the RGB color triplet [1/3 1/3 1/3] corresponding to a gray level. By referring to the reference image intensity image, as shown in Fig. 5.a, this representation allows us to better visualize the spatial evolution of the polarization state on the Poincaré's sphere (Fig. 5.c) or on the PQ projection (Fig. 5.e) as a function of the pixel location at the interface between three neighbouring grains. In addition, and as described previously, the boundary of the region of interest is distinguished by markers with a black edge.

Thus the first ROI shown in Fig.5.a is selected from a speckle pattern obtained on the partially depolarizing marble sample painted in green and is composed of three distinct grains. It can be seen on the Poincaré's sphere, and more particularly on the PQ projection, that these three grains have a circular polarimetric state (green markers), a vertical polarimetric state (blue markers) and a -45° polarimetric state, represented by the letter *M* (red markers). In this case, we are unable to visualize an organisation of polarization states in a form "enclosed" by the polarization states of the boundary. The field adopts a high diversity of states, with very rapid spatial evolution of the polarisation.

The second ROI, Fig.5.b, is obtained from a speckle pattern formed on the surface of the spectralon sample and is composed of a single *V*-shaped grain that we were able to fit into

a triangular ROI. We note in this case that, firstly, the distribution of polarization states on the surface of the Poincaré's sphere (Fig.5 d) and on the PQ map (Fig.5 f) is "denser" than in the previous case and, secondly, that the distribution of polarimetric states preserves the spatial distribution of the pixels. The polarimetric states appear to remain "enclosed" within the spatial distribution and remain within the polarization states located at the boundary of the ROI (represented by black border markers).

The two discussed examples show very distinct properties for the distribution of states across the Poincaré's sphere, the first one being very scattered over the entire sphere, while the second seems much more localized. We conjecture that the difference is due to the fact that the ROI of the first example encompasses a dark region in the intensity image. As a result, firstly, the level of confidence on the estimated SOPs is lower in such dark region, and secondly, it may happen that a field singularity lying in the triangular ROI leads to a very large spreading of the SOPs in the vicinity of the singularity, as will be observed and discussed in the next section.

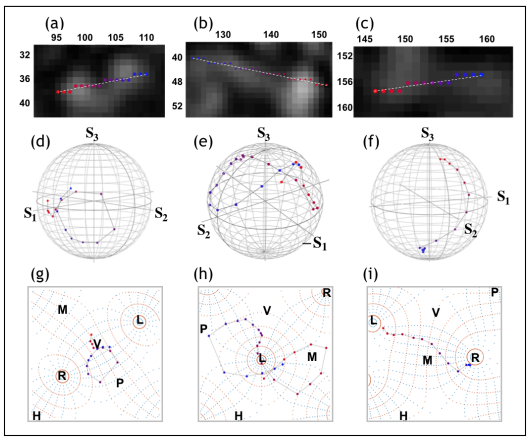

Fig. 6. First line: image of parameter S_0 with colored marking (from red to blue) of the pixels selected along a linear trajectory (dashed white line). Second line: representation of the selected pixels on the Poincaré's sphere, retaining the color coding of the markers. Third line: similar representation on the PQ projection.

Linear ROI In a previous work [3], a linear "trajectory of interest" on the images of the Stokes parameters, and in particular of S_0, was used to study the evolution of the polarization state between two grains or even within a single grain. In this seminal article, it was observed that the spatial evolution of the polarization state was continuous along such trajectory. In order to reproduce such results, we implemented a similar ROI by selecting the trajectory on the reference image S_0 (Fig.6.a, b and c), while assigning a colored marker (from red to blue, in RGB color encoding) to all the pixels located on this trajectory. Thus the pixels at each end are respectively assigned the RGB color code red $[1\ 0\ 0]$ and blue $[0\ 0\ 1]$ and the marker color code for the central pixel is purple $[1/2\ 0\ 1/2]$. As before, the sum of the RGB values is constrained to 1 and as this analysis is performed on a straight trajectory, the green colour is not used and its value remains zero. In addition, when we represent the corresponding SOPs on the Poincaré's sphere and on the PQ mapping, the color encoding of the SOPs links the points together by a continuous line corresponding to the spatial trajectory, thereby clearly guiding the reader through complex polarimetric evolution.

To visualize interesting evolutions of the SOP, we chose to study speckle patterns obtained from depolarizing samples such as Spectralon and green-painted brick. The three selected trajectories

shown in Fig.6.a-c were chosen to spatially link two adjacent speckle grains by a straight line. The results show that the evolution of the polarization state along a linear spatial trajectory (dashed white line) on the S_0 parameter images can represent a wide variety of trajectory shapes at the surface of the Poincaré's sphere and on the PQ projection map, as shown in Fig. 6 d-i. These trajectories represent a rather linear path from circular left (red markers) to circular right (blue markers) such as in Fig. 6.d and g; an "∞-shaped" trajectory such as in Fig. 6 e and h; or finally a loop-shaped trajectory such as in Fig. 6.f and i.

As observed in [3], the spatial evolution of the SOP is continuous, as these trajectories do not cross field singularities, but without a clearly repeatable trajectory structure, contrary to what could have been conjectured in [3]. It can be noted that, in order to check the validity of the experimental results presented here, it was verified that the DOP of the detected light along the selected trajectories is well preserved, as shown in Fig.7. The DOP along the trajectories is preserved and remains high (DOP > 0.75) for all ROIs (a), (b) and (c) which respectively correspond to the trajectories selected and displayed in Fig.6.a, b and c. Such verification confirms the validity of the experimental results presented in these figures, but these measurements do not reveal a clear trend in the behavior of the polarimetric trajectory at the transition between two neighboring speckle grains.

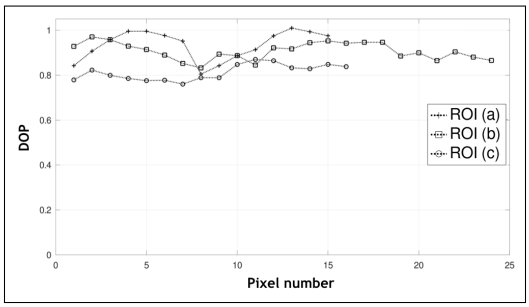

Fig. 7. DOP evolution along the selected linear path of the ROI displayed in Fig. 6.a-c

4.3. Single grain scale

The objective of this last representation for speckle polarimetric topology analysis is to provide a simple way to represent, as well as possible, the connexity between adjacent pixels on a Poincaré's sphere or on the corresponding PQ map, two representations that belong to the above-defined category of "spatial-structure-non-preserving representations". For that purpose, we proposed to introduce a spatial mesh on the pixels of the ROI (rectangular, polygonal or circular in shape) selected on the reference image S_0, as shown for instance in Fig. 8.a, b. This same mesh, referred to in the following as connexity mesh is then applied and plotted on the Poincaré's sphere (Fig. 8.c, d) or on the PQ map (Fig. 8.e, f) in order to "link" the SOPs represented depending on their spatial vicinity in the S_0 image.

To enhance the reader's understanding, the different edges of the selected polygonal ROI are assigned a distinct color, and vertical and horizontal lines of the mesh are represented in the projections by blue and red lines respectively. Finally, the color of the markers within the ROI is linked to the S_0 value, where high intensity is represented by a dark marker to enhance contrast with the white background of the Poincaré's sphere and PQ map. The results shown in Fig. 8 were obtained from speckle patterns produced on the Spectralon sample.

This representation, especially when projected on the PQ map, enables us to further analyze the above question, namely whether the SOPs within a chosen ROI delimiting a speckle grain remain (on the Poincaré's sphere and its PQ projection) within a region enclosed by he SOPs of the pixels of the edge of the spatial ROI, as was suggested in [3] and in Section 4.2. This

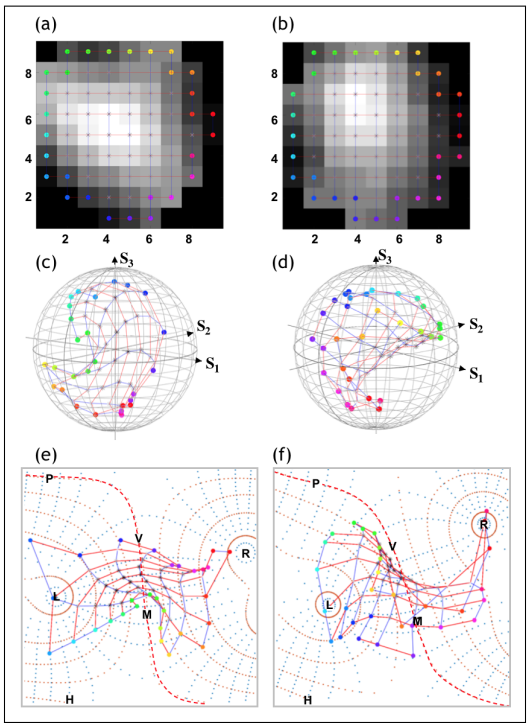

Fig. 8. First line: image of parameter S_0 for a Spectralon sample with a spatial mesh of selected pixels, where the markers corresponding to the boundary are colored. Second line: representation of the connexity mesh on the Poincaré's sphere of polarization states at each pixel. Third line: same representation on the PQ projection, where the equator of the Poincaré's sphere is highlighted with the dashed red line.

is sometimes the case, since we can see that the spatial mesh produced in Fig. 8.a retains its spatial structure when projected onto the Poincaré's sphere (Fig. 8.c and d) and the PQ map (Fig. 8.e and f), with a one-to-one correspondance between the pixel location and the SOP. The SOPs corresponding to the pixels inside the ROI indeed remain within the perimeter delimited by the SOPs of the pixels forming the ROI boundary. However, we observed on other grains that this situation is not a generality. Indeed, when projected onto the Poincaré's sphere and PQ representation, this spatial connexity mesh can "fold", allowing polarization states located inside the mesh to lie outside the perimeter formed by the polarization states corresponding to the ROI boundary, and there is no one-to-one correspondence between spatial location and SOP, as shown in the right column of Fig.8. This is an interesting observation for which, to our best knowledge, we do not have physical interpretation, but which could be the subject of further investigation in upcoming works.

Wether for the grain population, grain neighbourhood, or single grain analysis, for the sake of concision, only a small set of experimental "topological" analyses results have been presented here in this Section 4 among those that have been observed, focusing on a small number of cases. However, this study will need to be completed in subsequent work involving a large population of different grains and cases, in order to conduct a statistical analysis of the different situations observed. The automated experimental set-up developed and the data processing/analysis algorithms detailed in [1, 2] now offer this possibility with a high degree of confidence in the experimental results. In the last section of this paper, we will extend the analysis and the use of these proposed graphical tools to study the polarimetric behaviour of light at the vicinity of

polarization singularities.

5. Preferred representation for analyzing polarimetric singularities

Experimental and numerical studies of polarization singularities present in a speckle field have been the subject of many research studies [5, 20–23], finding more and more applications in very distinct domains such as super-resolved microscopy [24], or optical communications [25]. The kind of polarization singularities we will address below represent specific locations in the speckle field, characterized by non-zero intensity (i.e., not a field singularity) and a polarization state whose azimutal angle of the polarization ellipse is undefined, and in the vicinity of which the field exhibits extremely fast azimutal variations of the polarization ellipse (polarization state with a linear component). In this case three main configurations of polarization singularities are commonly identified [22] and referred to as "Lemon", "Star" and "Monstar", and can be described as follows (We refer the interested reader to [22] for further details):

- A Lemon-type singularity corresponds to lines of slow azimuth angle variations around a polarization ellipse line of constant azimuth
- A Star-type singularity corresponds to the intersection of three lines of constant azimuth, where the azimuth angle is zero at the point of singularity,
- A Monstar-type singularity is a hybrid situation between Lemon and Star singularities.

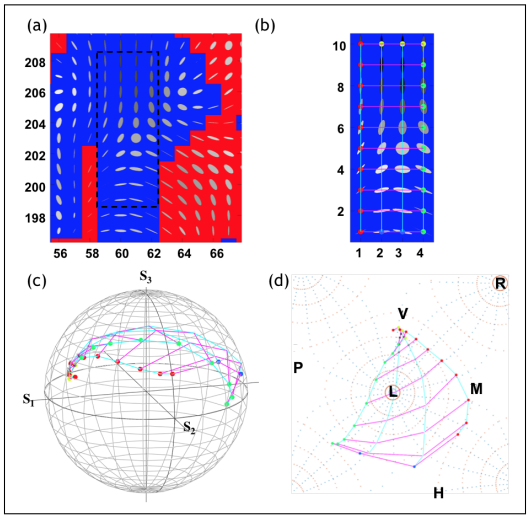

Fig. 9. (a) Star singularity observed in a speckle field produced with a Spectralon sample. Black dashed rectangular area: selected ROI. (b) Connexity mesh of pixels in the ROI. (c) Distribution of SOPs across the Poincaré's sphere displayed with connexity mesh. (d) Same as (c) for PQ projection.

To improve our understanding of the polarimetric evolution in the vicinity of a singularity, we rely on the previous representations and in particular the use of the connexity mesh as introduced in Section 4.3. Unlike previous representations, the ROI is represented on a reference image where the blue (red) colored background corresponds to a left (right) circular polarimetric state instead of the intensity S_0 image. As discussed in previous sections, a polarization ellipse is represented at each pixel location: the intensity (S_0) information is encoded by the brightness of the ellipse, where a white ellipse corresponds to a very bright pixel. As before, the DOP is

encoded by the size of the ellipse: hence, a state with a high DOP will be represented by a large ellipse size. This representation is shown for instance in Fig. 9.a, where a star singularity can be clearly identified in the center of the ROI.

The connexity mesh generated in this ROI and displayed in Fig. 9.b is then plotted on the Poincaré's sphere and on the PQ mapping (Fig. 9.c and d). Here, each side of the ROI has been associated with markers of the same color, and the vertical and horizontal lines of the mesh are identified by cyan/magenta colored lines. The Star singularity shown in Fig. 9 corresponds to the intersection of three trajectories whose azimuth angle varies slowly, and whose polarization state at the intersection is of indefinite azimuth (circular SOP), on which the ROI was centered. We note that the vertical linearly polarized states located on the top edge of the ROI (yellow markers) are all located close to the polarization state corresponding to the vertical state on the Poincaré's sphere $(1, 0, 0)$ (Fig. 9.c), and close to the V symbol on the PQ projection map (Fig. 9.d). The SOPs of pixels located along the left edge of the ROI spatially evolve towards a linear state close to $-45°$ (corresponding to point M on the (Fig. 9) and are represented with red markers. The pixels on the right edge of the ROI correspond to the green markers, and their SOPs evolve towards a linear state with an azimuth close to $+22.5°$ (located between the horizontal H state and the $+45°$ state marked P). Finally, the SOPs located along the ROI's central vertical axis vary from a vertical state to a near-horizontal state (H), transiting via a left-hand circular state (L). The mesh of this singularity is very insightful, particularly due to the fact that each of the three branches follows an evolution of the SOPs between linear polarization states: vertical state ($0°$ azimuth) (yellow markers), $-45°$ azimuth (intersection between blue and red markers) and $+22.5°$ azimuth (intersection between blue and green markers). Interestingly, this corresponds on the PQ projection to a rather triangular shape. The great advantage of Peirce's projection over the classical Poincaré's sphere mapping is obvious in this example: there is no ambiguity on Fig. 9.d to distinguish clearly the location of the SOPs, unlike in Fig. 9.c where it is difficult to distinguish whether the points are organized on the hemisphere facing the observer or on the opposite one. Next, we will focus on situations where two singularities are located close to each other, leading to interesting configurations of the SOP distribution.

5.1. Lemon-Monstar configuration

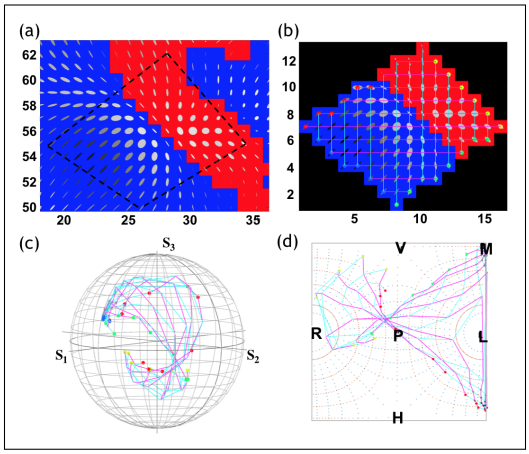

Fig. 10. (a) Lemon-Monstar configuration observed in a speckle field produced with a Spectralon sample. Black dashed polygonal area: selected ROI. (b) Mesh of selected pixels. (c) Distribution of SOPs across the Poincaré's sphere displayed with connexity mesh. (d) Same as (c) for PQ projection.

In this subsection, we first focus on an experimentally observed configuration of two singularities located in a close neighbourhood, namely a Lemon and a Monstar singularity (Fig. 10.a). As in the above subsection, a spatial mesh of the chosen polygonal ROI is produced and displayed in Fig. 10.b. The SOP at each pixel and the connexity mesh are plotted on the Poincaré's sphere and its PQ projection (Fig. 10.c and d).

It can be seen that in this configuration, all the horizontal lines of the mesh intersect, on the Poincaré's sphere and on the PQ projection, close to the linear polarimetric state of azimuth +45°. This intersection corresponds to the SOP of the pixels located at the frontier between positive (left-handed) ellipticity states (blue background in Fig. 10.b) and negative (right-handed) ellipticity states (red background). Once again, the proposed PQ projection associated to the connexity mesh displayed offers a very good readability of the spatial evolution to the SOP across the speckle field, and in the vicinity of polarization singularities.

5.2. Star-Star configuration

To end up this analysis of the topological distribution of SOPs around polarization singularities, let us focus on the experimentally observed Star-Star configuration, composed of the two Star singularities described above. This configuration shows a particularly interesting distribution of the SOPs, especially in the ROI displayed in Fig. 11.a.

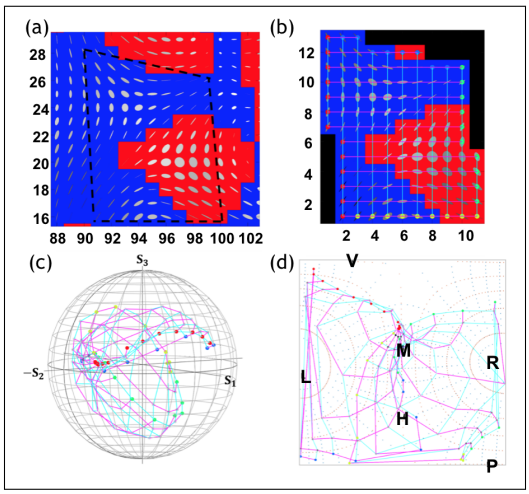

Fig. 11. Same as Fig. 10 for a Star-Star configuration of singularities.

This ROI can be basically split into two regions: a first upper triangle with positive (left-handed) ellipticity SOPs, and a second lower triangle with negative ellipticity SOPs. In such configuration of two Star polarization singularities in the vicinity of each other, the mapping of the SOPs across the Poincaré's sphere and on the PQ projection shows that such configuration tends to cover all possible SOPs. Indeed, the spatial mesh seems to spread over almost all the surface of the Poincaré's sphere (although with radius lower that unity, indicating partial polarization). The projection of this incomplete sphere onto the PQ is even clearer to demonstrate the fact that the observed SOPs almost cover all the surface of the PQ map. This interestingly shows that such Star-Star singularity configuration exhibits almost all possible polarimetric states in a very limited spatial extent on the imaged scene.

6. General conclusion and perspectives

This third part of the article series about "Optimized Stokes imaging for highly resolved optical speckle fields" has permitted to illustrate the wide variety of results and analyses that can be conducted when performing accurate Stokes imaging experiments on a speckle pattern, at a spatial scale such that the SOP of light can be mapped inside a single speckle grain. As discussed in this series, this was made possible by optimizing an experimental Stokes imaging setup in order to compensate carefully any source of bias or non-linearity in the measurement process, as detailed in the first article [1]. Furthermore, as we have established in the second article [2], the performance of such polarimetric imaging experiment has been optimized, in terms of accuracy, precision and robustness to experimental imperfections, by resorting to the so-called SOPAFP approach, using appropriate polarization analysis states, which enabled us to provide the experimental results presented in the present article.

In order to complete this study and provide the reader with useful tools in the particular context of this study, we have also introduced and discussed various ways of representing and analyzing the polarimetric data. In the context of imaging the SOPs on a speckle pattern, we have shown that using a particular planispheric projection of the SOPs on the Poincaré's sphere, namely the Peirce's quicuncial projection, appears to be a very interesting approach to enhance the readability of such results and to help in the analysis of the spatial behaviour of the distribution of SOPs. In particular, we have demonstrated the benefit of the PQ projection over the Poincaré's sphere representation in order to avoid confusion or occultation of SOPs when the SOPs distribution tends to occupy the entire sphere. Lastly, based on these general modalities, we have proposed several refined graphical representations, adapted to various scales of observation ("macroscopic" analysis, population of a few grains, interface between neighbouring grains, and finally single grain), and to different "topological" properties that can be investigated on the spatial distribution of SOPs across a speckle field. In all cases, the objective is to preserved at best the spatial information (even though it is naturally lost in representations such as Poincaré's sphere or PQ projection), but resorting to colored markers, or connexity meshes... In addition, we were also able to observe polarization singularities of various kinds, and to analyze their spatial distributions with optimized graphical tools.

This study thus provides a complete review of the optimal methodology to perform polarimetric state metrology at the speckle grain scale, from the experimental device to the processing and estimation strategies, as well as original representations of the polarimetric information. With such automated and optimized experiment, we are now able to conduct extensive investigations of the polarization properties of speckle fields. This work opens many perspectives, mainly experimental, but which could provide interesting insights to open theoretical questions that are still pending in the domain. In particular, it will be very interesting to analyze the evolution of the SOPs distribution with modification of the physical properties of the illumination laser, such as tuning the wavelength, the coherence properties of the source, and/or modifying the DOP of the illumination beam ranging from fully polarized to totally unpolarized.

These experiments and this optimized setup also paves the way to experimental measurement of original depolarization metrics proposed in the field of statistical optics that could be very interesting to investigate on a speckle pattern, which could lead to identify and measure more subtle statistical descriptors of light depolarization, such as non-isotropic and/or non-gaussian depolarization processes, already proposed theoretically [26] but to be observed experimentally. Another class of interesting parameters could be the second-order (two-point) polarimetric statistics (such as two-point DOP, or two-point Stokes parameters [27, 28]) which could enable the definition of a "spatial polarization coherence", and somehow be linked to less standard spatial coherence properties [29, 30]. Identifying specific samples or materials that could lead to particular spatial depolarization patterns across the speckle field (such as an anisotropic spatial depolarization) is another perspective to this work. Combined with the non-standard descriptors of light properties mentioned above, original polarization metrology approaches such as the

one described in this work could also exhibit an interest for applications: they could indeed give relevant clues to discriminate materials sharing identical "macroscopic" characteristics (spectrum, degree of polarization;. . .) but which could differ in terms of the internal structural properties of their SOPs distribution.

Acknowledgments. The authors would like to thank the DOP team of Institut Foton for fruitful discussions, as well as F. Théry and F. Murie for insightful debates on the mental representation of polarimetric information.

Disclosures. The authors declare no conflicts of interest.

Data availability. Data underlying the results presented in this paper are not publicly available at this time but may be obtained from the authors upon reasonable request.

References

1. J. Staes and J. Fade, "Optimized stokes imaging for highly resolved optical speckle fields, part I: Optimized experimental setup," submitted to J. Opt. Soc. Am. A (2024).
2. J. Staes and J. Fade, "Optimized stokes imaging for highly resolved optical speckle fields, part II: Optimal acquisition & estimation strategies," submitted to J. Opt. Soc. Am. A (2024).
3. L. Pouget, J. Fade, C. Hamel, and M. Alouini, "Polarimetric imaging beyond the speckle grain scale," Appl. optics **51**, 7345–7356 (2012).
4. M. Zerrad, H. Tortel, G. Soriano, A. Ghabbach, and C. Amra, "Spatial depolarization of light from the bulks: electromagnetic prediction," Opt. Express **23**, 8246–8260 (2015).
5. J. Dupont, X. Orlik, R. Ceolato, and T. Dartigalongue, "Spectralon spatial depolarization: towards an intrinsic characterization using a novel phase shift distribution analysis," Opt. Express **25**, 9544–9555 (2017).
6. D. Haner and B. McGuckin, "Measurement of the depolarization of reflected light from spectralon," Appl. Opt. (1997).
7. Ø. Svensen, M. Kildemo, J. Maria, J. J. Stamnes, and Ø. Frette, "Mueller matrix measurements and modeling pertaining to spectralon white reflectance standards," Opt. express **20**, 15045–15053 (2012).
8. J. M. Sanz, C. Extremiana, and J. Saiz, "Comprehensive polarimetric analysis of spectralon white reflectance standard in a wide visible range," Appl. optics **52**, 6051–6062 (2013).
9. C. J. Bruegge, A. E. Stiegman, R. A. Rainen, and A. W. Springsteen, "Use of spectralon as a diffuse reflectance standard for in-flight calibration of earth-orbiting sensors," Opt. Eng. **32**, 805–814 (1993).
10. R. D. Jackson, T. R. Clarke, and M. S. Moran, "Bidirectional calibration results for 11 spectralon and 16 baso4 reference reflectance panels," Remote. sensing environment **40**, 231–239 (1992).
11. M. J. Choi, S. R. Guntur, K. I. Lee, D. G. Paeng, and A. Coleman, "A tissue mimicking polyacrylamide hydrogel phantom for visualizing thermal lesions generated by high intensity focused ultrasound," Ultrasound medicine & biology **39**, 439–448 (2013).
12. C. Kim, A. Garcia-Uribe, S.-R. Kothapalli, and L. V. Wang, "Optical phantoms for ultrasound-modulated optical tomography," in *Design and Performance Validation of Phantoms Used in Conjunction with Optical Measurements of Tissue,* vol. 6870 (SPIE, 2008), pp. 147–154.
13. J. Dupont and X. Orlik, "Polarized vortices in optical speckle field: observation of rare polarization singularities," Opt. express **23**, 6041–6049 (2015).
14. A. Ghabbach, M. Zerrad, G. Soriano, and C. Amra, "Accurate metrology of polarization curves measured at the speckle size of visible light scattering," Opt. Express **22**, 14594–14609 (2014).
15. J. Tyo, E. Pugh, and N. Engheta, "Colorimetric representations for use with polarization-difference imaging of objects in scattering media," JOSA A **15**, 367–374 (1998).
16. K. M. Yemelyanov, S.-S. Lin, W. Q. Luis, E. N. Pugh Jr, and N. Engheta, "Bio-inspired display of polarization information using selected visual cues," in *Polarization Science and Remote Sensing,* vol. 5158 (SPIE, 2003), pp. 71–84.
17. K. M. Yemelyanov, M. Lo, E. Pugh, and N. Engheta, "Display of polarization information by coherently moving dots," Opt. Express **11**, 1577–1584 (2003).
18. A. M. Beckley, T. G. Brown, and M. A. Alonso, "Full poincaré beams," Opt. express **18**, 10777–10785 (2010).
19. C. S. Peirce, "A quincuncial projection of the sphere," Am. J. Math. **2**, 394–396 (1879).
20. D. Ye, X. Peng, Q. Zhao, and Y. Chen, "Numerical generation of a polarization singularity array with modulated amplitude and phase," JOSA A **33**, 1705–1709 (2016).
21. B. Kumar, P. Lochab, E. Baidya Kayal, D. P. Ghai, P. Senthilkumaran, and K. Khare, "Speckle in polarization structured light," J. Mod. Opt. **69**, 47–54 (2022).

22. F. Flossmann, O. Kevin, M. R. Dennis, and M. J. Padgett, "Polarization singularities in 2d and 3d speckle fields," Phys. review letters **100**, 203902 (2008).
23. M. S. Soskin, V. G. Denisenko, and R. I. Egorov, "Singular stokes-polarimetry as new technique for metrology and inspection of polarized speckle fields," in *Optical Micro-and Nanometrology in Manufacturing Technology,* vol. 5458 (SPIE, 2004), pp. 79–85.
24. M. Pascucci, G. Tessier, V. Emiliani, and M. Guillon, "Superresolution imaging of optical vortices in a speckle pattern," Phys. review letters **116**, 093904 (2016).
25. J. Wang, J.-Y. Yang, I. M. Fazal, N. Ahmed, Y. Yan, H. Huang, Y. Ren, Y. Yue, S. Dolinar, M. Tur *et al.*, "Terabit free-space data transmission employing orbital angular momentum multiplexing," Nat. photonics **6**, 488–496 (2012).
26. P. Réfrégier, "Polarization degree of optical waves with non gaussian probability density functions: Kullback relative entropy-based approach," Opt. Lett. **30**, 1090–1092 (2005).
27. O. Korotkova and E. Wolf, "Generalized stokes parameters of random electromagnetic beams," Opt. Lett. **30**, 198–200 (2005).
28. J. Tervo, T. Setälä, A. Roueff, P. Réfrégier, and A. T. Friberg, "Two-point stokes parameters: interpretation and properties," Opt. Lett. **34**, 3074–3076 (2009).
29. A. Gautam, G. Arora, P. Senthilkumaran, and R. K. Singh, "Detecting topological index of randomly scattered v-point singularities using stokes correlations," JOSA A **41**, 95–103 (2024).
30. P. Réfrégier and J. Fade, "Polarization coherence frustration," submitted to J. Opt. Soc. Am. A (2024).